Supplementary Information

Multicolour Barcoding in One MOF Crystal Through Rationally Postsynthetic Transmetalation

Weilinsen Ding, Lina Zhao, Xiaoyun Yuan, Lantian Zhang, Baojun Chen, Qiang Ju* and Zhenlan Fang*

Table of Contents

1. Tables

1.1 Table S1 (Crystal Data and Structure Refinement Results for ***IAM19-1*****)**

1.2 Table S2 (Selected Bond Lengths (Å) and Angles (°) for ***IAM19-1*****)**

2. Figures

1) Nitrogen Adsorption and Desorption Isotherms (Figure S1)

2) PXRD Patterns and Crystallographic Data (Figure S2-S5, Figure S16)

2.1 PXRD patterns of ***IAM19-1*** (Ce^{3+}-MOF).

2.2 PXRD patterns of ***IAM19-1a*** (Tb^{3+}, Ce^{3+}-MOF).

2.3 PXRD patterns of ***IAM19-1b*** (Eu^{3+}, Ce^{3+}-MOF).

2.4 PXRD patterns of ***IAM19-1c*** (Eu^{3+}, Ce^{3+}@Tb^{3+}, Ce^{3+}-MOF).

2.5 PXRD patterns of activated ***IAM19-1*** (Ce^{3+}-MOF)

3) IR-Spectroscopy (Figure S6)

4) Optical Properties (Figure S7-S15, S17-S21)

4.1 Decay curves of ***IAM19-1a*** (Tb^{3+}, Ce^{3+}-MOF), and ***IAM19-1b*** (Eu^{3+}, Ce^{3+}-MOF).

4.2 The emission spectra of ***IAM19-1*** (Ce^{3+}-MOF).

4.3 Emission spectra of ***IAM19-1a*** when ***IAM19-1*** was immersed in Eu^{3+} solution at different temperature, different time, different concentration, and different solvent.

4.4 Excitation and emission spectra of ***IAM19-1a*** (Tb^{3+}, Ce^{3+}-MOF), ***IAM19-1b*** (Eu^{3+}, Ce^{3+}-MOF), and ***IAM19-1c*** (Eu^{3+}, Ce^{3+}@Tb^{3+}, Ce^{3+}-MOF).

4.5 The emission photography of ***IAM19-1a***, ***IAM19-1b***, ***IAM19-1c*** and ***IAM19-1c'***.

4.6 The fabrication procedure for ***IAM19-1c*** and ***IAM19-1c'.***

5）Thermogravimetric Analysis (Figure S22-S24)

5.1 Thermogravimetric analysis of ***IAM19-1*** (Ce^{3+}-MOF) and ***IAM19-1a*** (Tb^{3+}, Ce^{3+}-MOF).

5.2 Thermogravimetric analysis of ***IAM19-1*** (Ce^{3+}-MOF) and ***IAM19-1b*** (Eu^{3+}, Ce^{3+}-MOF).

5.3 Thermogravimetric analysis of ***IAM19-1*** (Ce^{3+}-MOF) and ***IAM19-1c*** (Eu^{3+}, Ce^{3+}@Tb^{3+}, Ce^{3+}-MOF).

Table S1. Crystal Data and Structure Refinement Results for ***IAM19-1***

MOF	***IAM19-1***
empirical formula	$Ce_4C_{84}H_{64}O_{37}$
formula weight	2225.80
crystal system	Monoclinic
space group	*P*21/c
Z	2
a (Å)	13.576(2)
b (Å)	29.448(3)
c (Å)	9.523(1)
α (deg)	90
β (deg)	93.152(3)
γ (deg)	90
V (Å^3)	3801.3(7)
ρ_{calcd} (g/cm^3)	1.941
μ (mm^{-1})	2.452
temp (K)	295
GOF	1.043
R_1 (I>2σ(I))[a]	0.046
wR_2 (I>2σ(I))[a]	0.186
R_1 (all data)[b]	0.062
wR_2 (all data)[b]	0.202

[a] $R_1 = \sum||F_o| - |F_c||/\sum|F_o|$; [b] $wR_2 = \{\sum[w(F_o^2 - F_c^2)^2/\sum[w(F_o^2)^2]]\}^{1/2}$

Table S2. Selected Bond Lengths (Å) and Angles (°) for ***IAM19-1***

Ce(1)-O(1)	2.436(3)	Ce(1)-O(16)	2.518(4)
Ce(1)-O(4)#1	2.457(3)	Ce(1)-O(14)#4	2.560(4)
Ce(1)-O(15)#2	2.460(4)	Ce(1)-O(17)	2.723(4)
Ce(1)-O(5)#3	2.465(4)	Ce(1)-O(4)#3	2.743(3)
Ce(1)-O(11)	2.475(4)	Ce(1)-Ce(1)#5	4.0599(7)
Ce(2)-O(12)	2.424(3)	Ce(2)-O(10)#7	2.519(4)
Ce(2)-O(6)	2.436(4)	Ce(2)-O(18)	2.610(6)
Ce(2)-O(2)	2.453(4)	Ce(2)-O(17)	2.755(4)
Ce(2)-O(9)#3	2.476(4)	Ce(2)-O(6)#6	2.891(4)
Ce(2)-O(7)#6	2.484(4)	Ce(2)-Ce(2)#6	4.0716(8)
O(1)-Ce(1)-O(4)#1	145.33(12)	O(15)#2-Ce(1)-O(5)#3	80.77(13)
O(1)-Ce(1)-O(15)#2	137.38(12)	O(1)-Ce(1)-O(11)	91.39(12)
O(4)#1-Ce(1)-O(15)#2	76.17(12)	O(4)#1-Ce(1)-O(11)	86.86(12)
O(1)-Ce(1)-O(5)#3	76.69(12)	O(15)#2-Ce(1)-O(11)	79.14(14)
O(4)#1-Ce(1)-O(5)#3	126.99(11)	O(5)#3-Ce(1)-O(11)	134.26(12)
O(1)-Ce(1)-O(16)	72.12(13)	O(1)-Ce(1)-O(14)#4	79.91(12)
O(4)#1-Ce(1)-O(16)	74.17(12)	O(4)#1-Ce(1)-O(14)#4	81.14(12)
O(15)#2-Ce(1)-O(16)	140.51(13)	O(15)#2-Ce(1)-O(14)#4	129.93(12)
O(5)#3-Ce(1)-O(16)	138.44(13)	O(5)#3-Ce(1)-O(14)#4	78.38(12)
O(11)-Ce(1)-O(16)	73.79(13)	O(11)-Ce(1)-O(14)#4	143.48(13)
O(16)-Ce(1)-O(14)#4	69.77(13)	O(11)-Ce(1)-O(17)	69.20(12)
O(1)-Ce(1)-O(17)	71.08(12)	O(16)-Ce(1)-O(17)	126.09(14)
O(4)#1-Ce(1)-O(17)	138.59(11)	O(14)#4-Ce(1)-O(17)	137.32(11)
O(15)#2-Ce(1)-O(17)	66.69(13)	O(1)-Ce(1)-O(4)#3	118.34(11)
O(5)#3-Ce(1)-O(17)	65.13(11)	O(4)#1-Ce(1)-O(4)#3	77.50(12)
O(15)#2-Ce(1)-O(4)#3	68.14(12)	O(17)-Ce(1)-O(4)#3	103.73(12)
O(5)#3-Ce(1)-O(4)#3	49.58(11)	O(12)-Ce(2)-O(6)	147.21(13)
O(11)-Ce(1)-O(4)#3	146.18(12)	O(12)-Ce(2)-O(2)	90.51(12)
O(16)-Ce(1)-O(4)#3	128.20(12)	O(6)-Ce(2)-O(2)	85.23(13)
O(14)#4-Ce(1)-O(4)#3	63.62(11)	O(12)-Ce(2)-O(9)#3	135.12(13)
O(6)-Ce(2)-O(9)#3	75.54(14)	O(9)#3-Ce(2)-O(7)#6	81.14(14)
O(2)-Ce(2)-O(9)#3	77.67(15)	O(12)-Ce(2)-O(10)#7	81.57(12)
O(12)-Ce(2)-O(7)#6	76.50(12)	O(6)-Ce(2)-O(10)#7	83.89(13)
O(6)-Ce(2)-O(7)#6	128.03(13)	O(2)-Ce(2)-O(10)#7	145.77(15)
O(2)-Ce(2)-O(7)#6	133.76(14)	O(9)#3-Ce(2)-O(10)#7	129.99(14)
O(7)#6-Ce(2)-O(10)#7	76.71(14)	O(7)#6-Ce(2)-O(18)	140.00(17)
O(12)-Ce(2)-O(18)	74.14(15)	O(10)#7-Ce(2)-O(18)	72.65(17)
O(6)-Ce(2)-O(18)	73.52(16)	O(12)-Ce(2)-O(17)	70.02(12)
O(2)-Ce(2)-O(18)	73.15(17)	O(6)-Ce(2)-O(17)	136.66(12)
O(9)#3-Ce(2)-O(18)	138.70(17)	O(2)-Ce(2)-O(17)	69.47(12)
O(9)#3-Ce(2)-O(17)	65.26(13)	O(6)-Ce(2)-O(6)#6	80.66(13)
O(7)#6-Ce(2)-O(17)	64.35(12)	O(2)-Ce(2)-O(6)#6	145.59(13)
O(10)#7-Ce(2)-O(17)	135.76(12)	O(9)#3-Ce(2)-O(6)#6	68.48(13)
O(18)-Ce(2)-O(17)	126.96(14)	O(7)#6-Ce(2)-O(6)#6	47.51(11)
O(12)-Ce(2)-O(6)#6	117.73(11)	O(10)#7-Ce(2)-O(6)#6	63.42(13)
O(18)-Ce(2)-O(6)#6	130.80(14)	O(17)-Ce(2)-O(6)#6	100.52(12)

Symmetry transformations used to generate equivalent atoms:

IAM19-1, (#1) -x, y-1/2, -z+3/2; (#2) x, -y-1/2, z+1/2; (#3) x, -y+1/2, z+1/2; (#4) -x, y+1/2, -z+3/2; (#5) -x, -y, -z+2; (#6) -x+1, -y, -z+1; (#7) -x+1, y-1/2, -z+1/2; (#8) x, -y+1/2, z-1/2; (#9) -x+1, y+1/2, -z+1/2; (#10) x, -y-1/2, z-1/2.

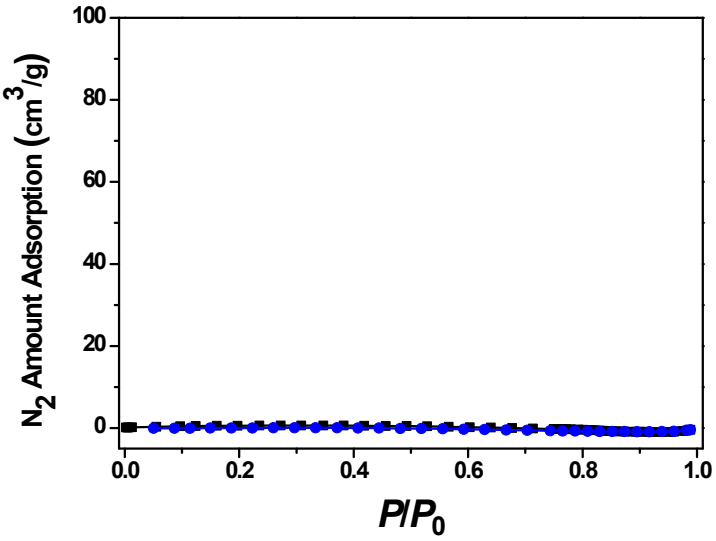

Figure S1. Nitrogen adsorption (blue line) and desorption (black line) isotherms for ***IAM19-1*** after thermal activation at 280 °C for 12 hours.

It indicates that no available idle space is presented in the activated ***IAM19-1*** after removing the free and coordinated water molecules.

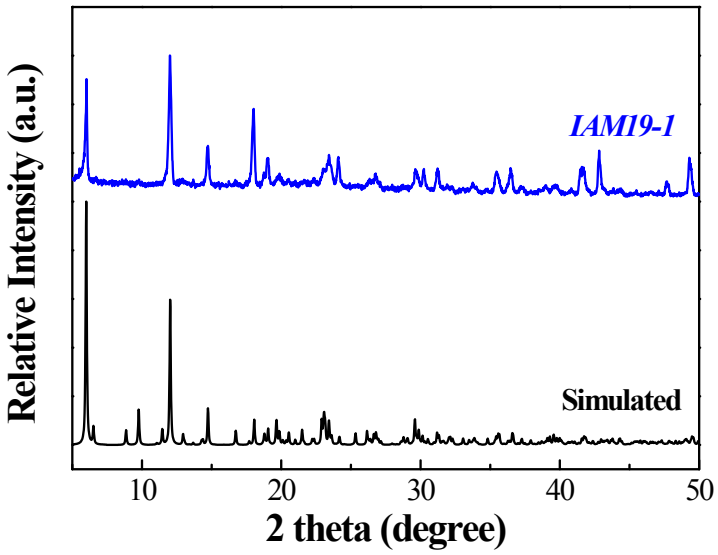

Figure S2. The powder X-ray diffraction pattern of ***IAM19-1*** and simulated pattern from a single crystal of ***IAM19-1***.

The powder X-ray diffraction pattern of as-synthesized ***IAM19-1*** matches well with that of simulated from the CIF file of an ***IAM19-1*** single crystal, demonstrating that the as-synthesized ***IAM19-1*** sample is pure.

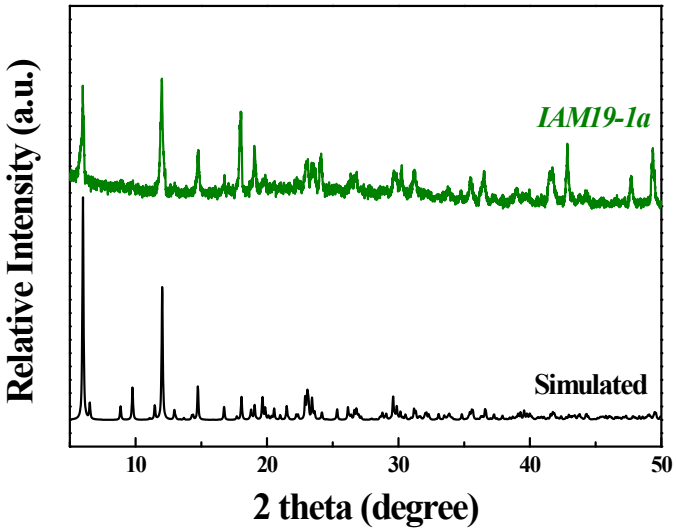

Figure S3. The powder X-ray diffraction pattern of ***IAM19-1a*** and the simulated X-ray diffraction pattern from a single crystal of ***IAM19-1***.

The powder X-ray diffraction pattern of as-synthesized ***IAM19-1a*** matches well with that of simulated from the CIF file of an ***IAM19-1*** single crystal, demonstrating that the as-synthesized ***IAM19-1a*** sample is pure, and maintains the framework of parent ***IAM19-1***.

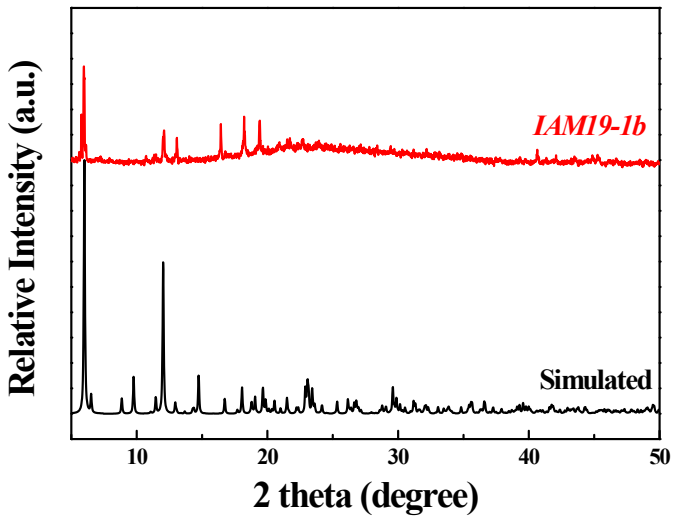

Figure S4. The powder X-ray diffraction pattern of ***IAM19-1b*** and the simulated powder X-ray diffraction pattern from a single crystal of ***IAM19-1***.

The powder X-ray diffraction pattern of as-synthesized ***IAM19-1b*** matches well with that of simulated from the CIF file of an ***IAM19-1*** single crystal, demonstrating that the as-synthesized ***IAM19-1b*** sample is pure, and maintains the framework of parent ***IAM19-1***.

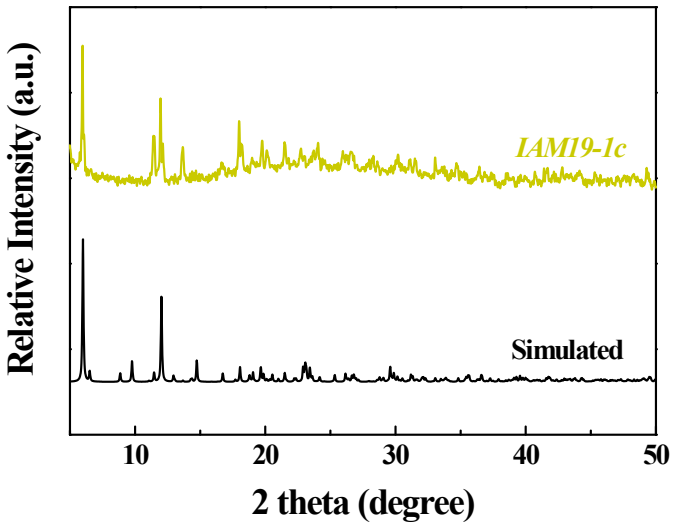

Figure S5. The powder X-ray diffraction pattern of ***IAM19-1c*** and the simulated powder X-ray diffraction pattern from a single crystal of ***IAM19-1***.

The powder X-ray diffraction pattern of as-synthesized ***IAM19-1c*** matches well with that of simulated from the CIF file of an ***IAM19-1*** single crystal, demonstrating that the as-synthesized ***IAM19-1c*** sample is pure, and maintains the framework of parent ***IAM19-1***.

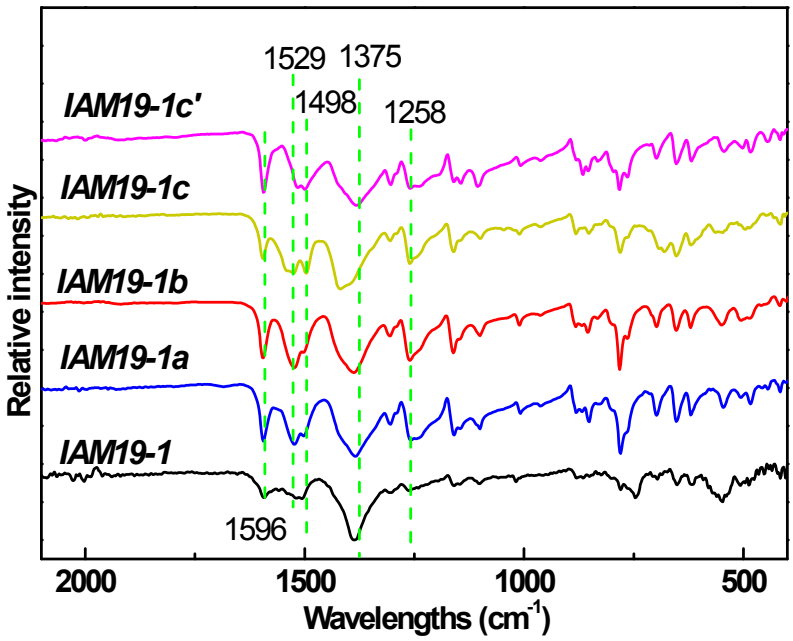

Figure S6. FT-IR spectra of ***IAM19-1*** (black), ***IAM19-1a*** (blue), ***IAM19-1b*** (red), ***IAM19-1c*** (yellow), and ***IAM19-1c'*** (pink).

The band centered at ~1596, ~1529-1498, ~1375 and ~1258 cm^{-1} can be attributed to the asymmetrical C=O stretching mode of carboxylate group, C=C stretching mode of benzene ring, symmetrical C=O stretching mode of carboxylate group, and C-O stretching of aromatic ether, respectively. The high similarity of the parent Ce-MOF ***IAM19-1*** and all the other derived luminescent MOFs further demonstrates the postsynthetic MOFs maintain the framework of parent Ce-MOF. Compared with ***IAM19-1***, the band shifts and changes of relative intensity in the FT-IR spectra of ***IAM19-1a***, ***IAM19-1b***, ***IAM19-1c***, ***IAM19-1c'*** primarily result from the incorporation of Eu^{3+}, Tb^{3+} or both.

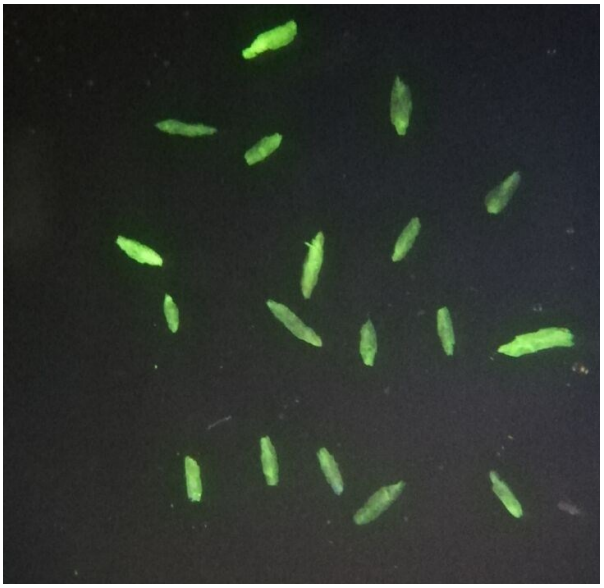

Figure S7. Photography of green luminescent ***IAM19-1a*** (Tb^{3+}, Ce^{3+}-MOF) obtained from single crystal after PSTM under irradiation at 254 nm with a 4 W hand-held UV lamp.

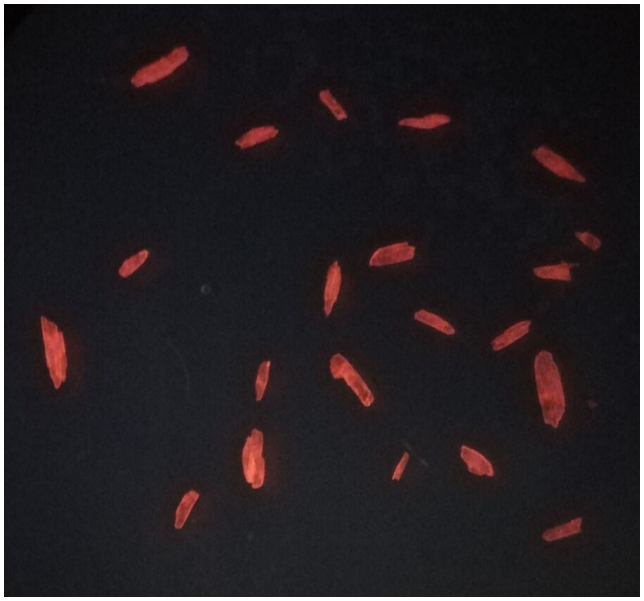

Figure S8. Photography of red luminescent ***IAM19-1b*** (Eu^{3+}, Ce^{3+}-MOF) obtained from single crystal after PSTM under irradiation at 254 nm with a 4 W hand-held UV lamp.

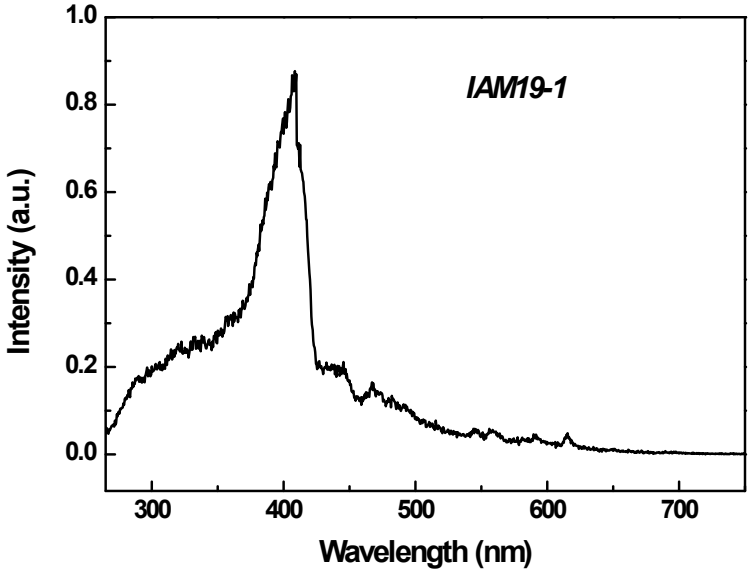

Figure S9. Emission spectra of ***IAM19-1*** under the excitation of 254 nm.

The intensity of ***IAM19-1*** is only one percentage of that of ***IAM19-1a*** and ***IAM19-1b*** under the same condition. Therefore, the emission of Ce^{3+} is difficult to be detected out in the ***IAM19-1a***, ***IAM19-1b***, ***IAM19-1c***, ***IAM19-1c'***.

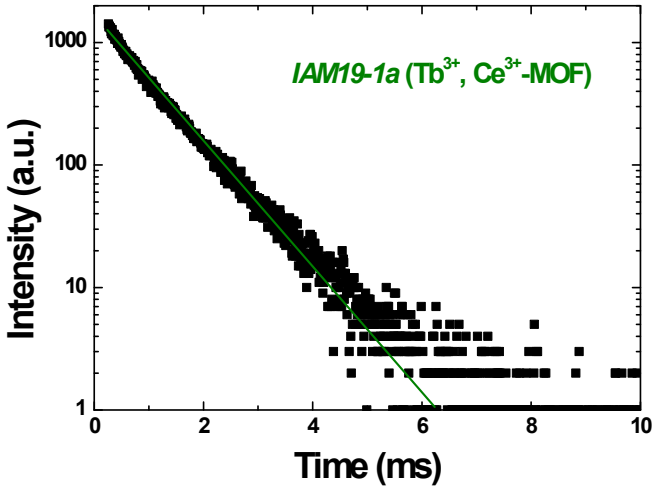

Figure S10. Photoluminescent decay from $^5D_4$ of Tb^{3+} in ***IAM19-1a*** under excitation at 254 nm.

The green line represents the profile fitted by single-exponential function, which shows a lifetime to be 0.74 ms.

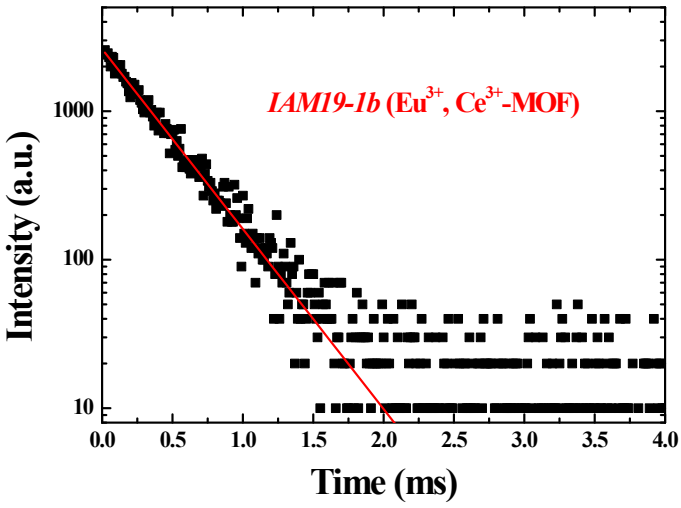

Figure S11. Photoluminescent decay from $^5D_0$ of Eu^{3+} in ***IAM19-1b*** under excitation at 254 nm.
The red line represents the profile fitted by single-exponential function, which shows a lifetime to be 0.35 ms.

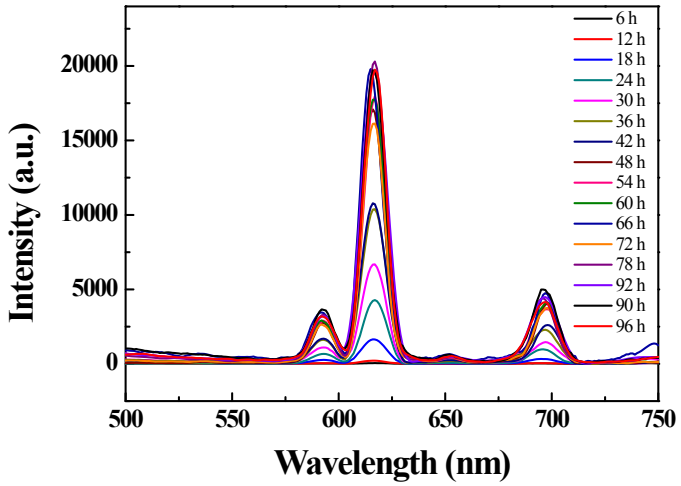

Figure S12. Emission spectra of ***IAM19-1b*** when ***IAM19-1*** was immersed in Eu^{3+} aqueous solution (0.2 M) at 80 °C for different time under excitation at 254 nm.

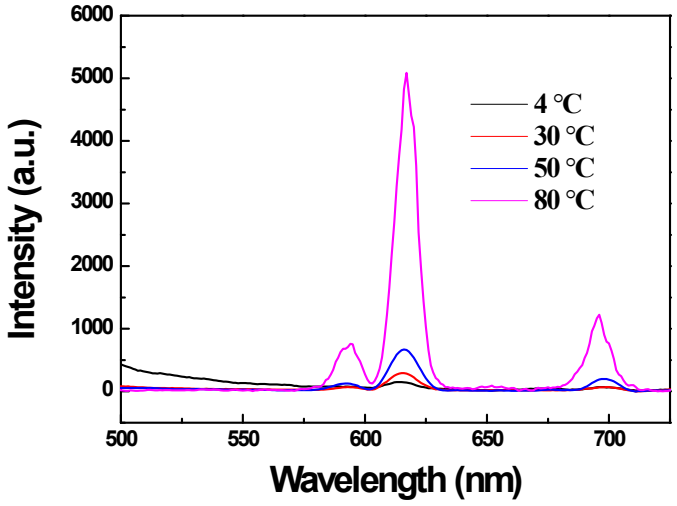

Figure S13. Emission spectra of ***IAM19-1a*** when ***IAM19-1*** was immersed in Eu^{3+} aqueous solution (0.2 M) for 20 hours at different temperature under excitation at 254 nm.

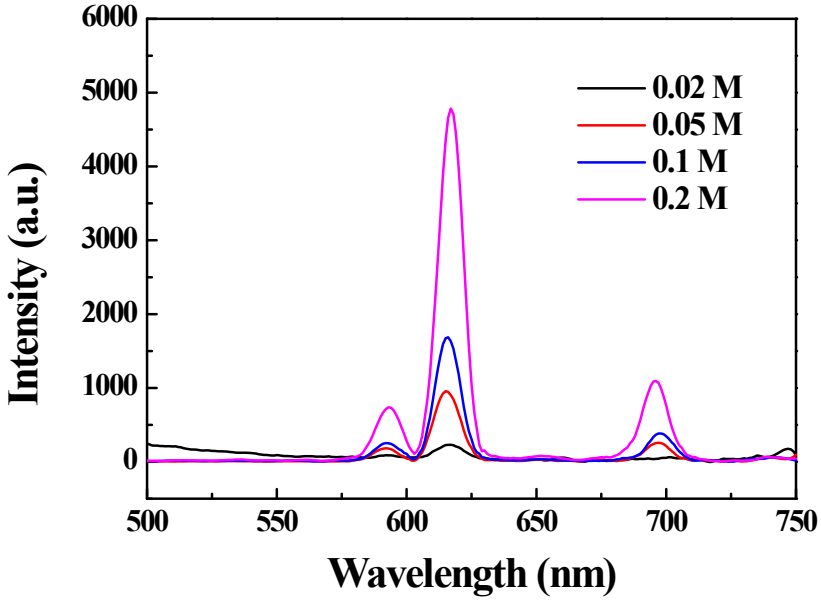

Figure S14. Emission spectra of ***IAM19-1b*** when ***IAM19-1*** was immersed in Eu^{3+} aqueous solution for 24 hours at 80 °C at different concentrations under excitation at 254 nm.

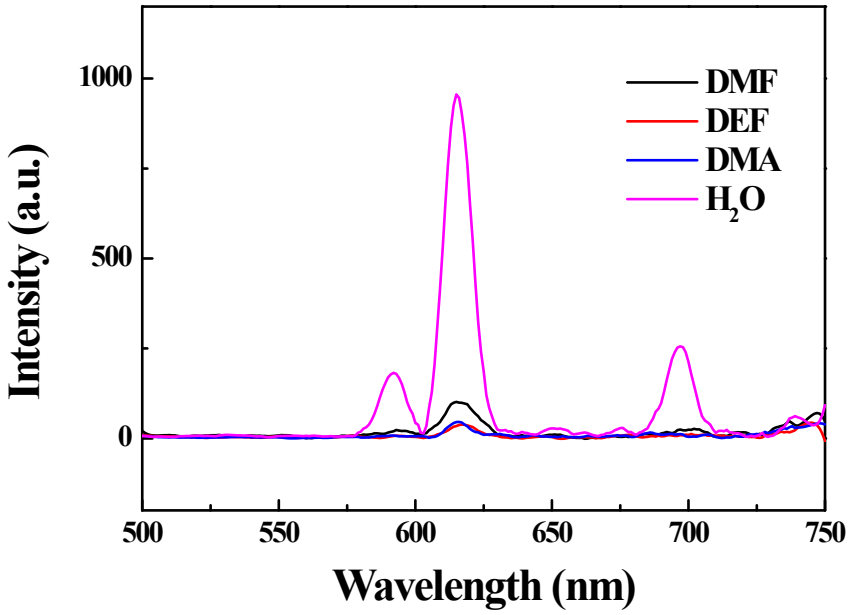

Figure S15. Emission spectra of ***IAM19-1b*** when ***IAM19-1*** was immersed in Eu^{3+} solution (0.05 M) for 24 hours at 80 °C in different solvents under excitation at 254 nm.

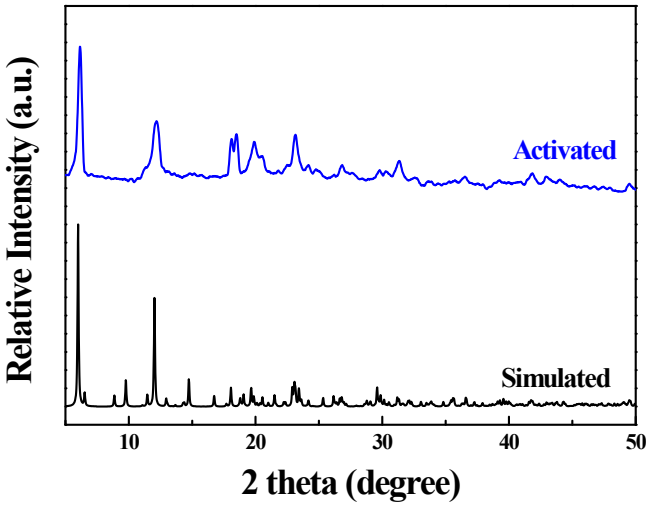

Figure S16. The comparison of the measured powder X-ray diffraction pattern of ***IAM19-1*** after activation 280 °C for 12 hours with the simulated powder X-ray diffraction pattern obtained from a single crystal of ***IAM19-1***.

The result demonstrates that the activated sample is pure and it maintains the framework of ***IAM19-1*** after activation.

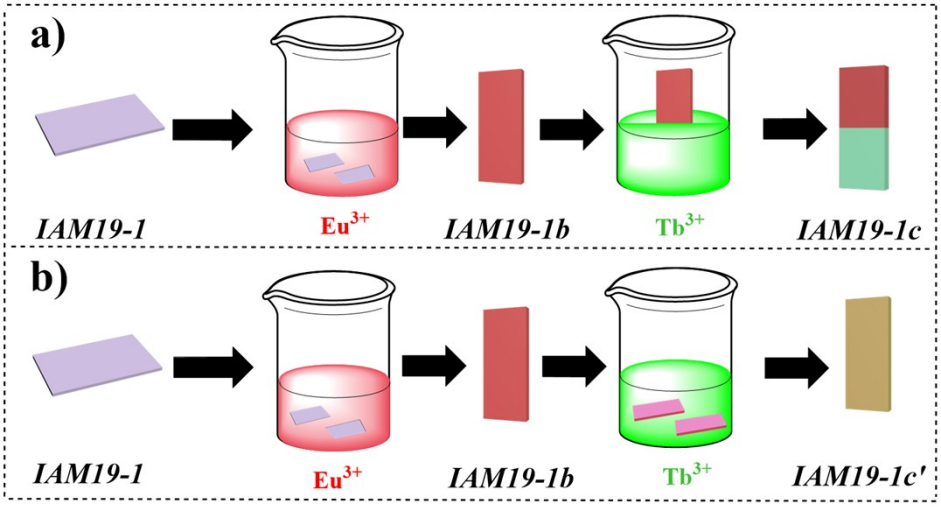

Figure S17. Schematic diagram illustrating the PSTM procedure for producing a) dual-emissive ***IAM19-1c*** and b) homogeneous ***IAM19-1c'***.

When one end of ***IAM19-1b*** was dipped into Tb^{3+} solution, the dual-emissive one-crystal ***IAM19-1c*** was formed, while when ***IAM19-1b*** was completely immersed in Tb^{3+} solution, the homogeneous yellow luminescent ***IAM19-1c'*** can be obtained.

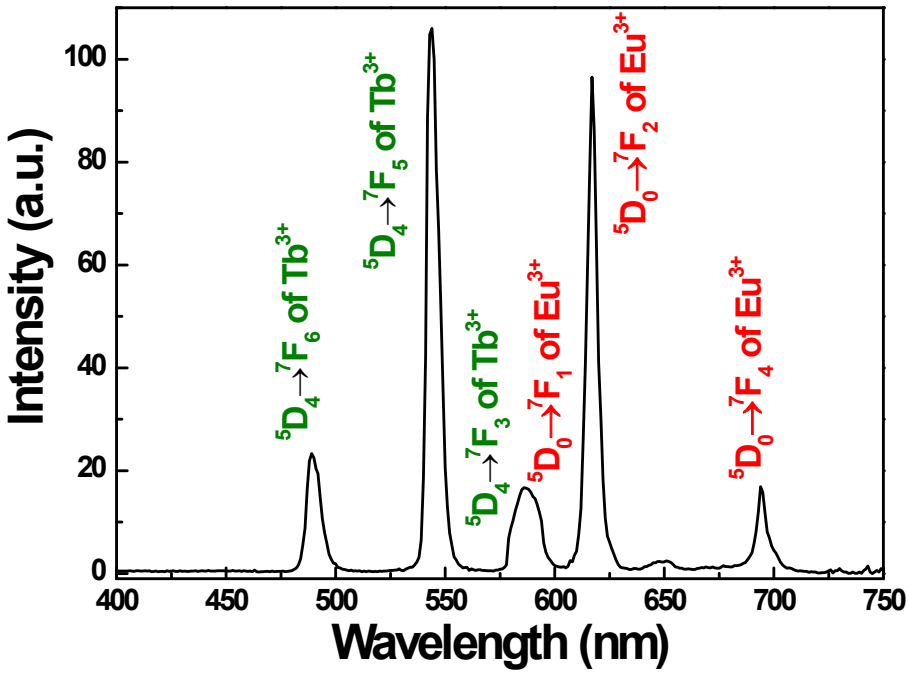

Figure S18. Emission spectra of ***IAM19-1c*** under the excitation of 254 nm.

It unambiguously proves the presence of both Tb^{3+} and Eu^{3+} in ***IAM19-1c*** MOFs.

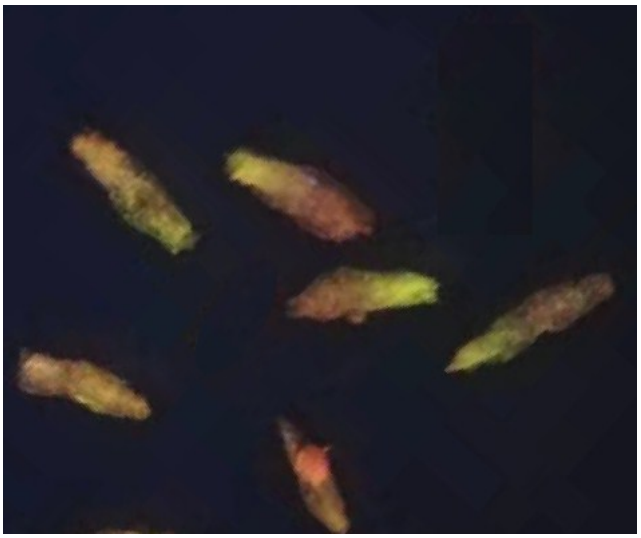

Figure S19. Photography of dual-emissive (red@green) ***IAM19-1c*** (Eu^{3+}, Ce^{3+}@Tb^{3+}, Ce^{3+}-MOF) taken by ordinary microscope under the excitation of 254 nm.

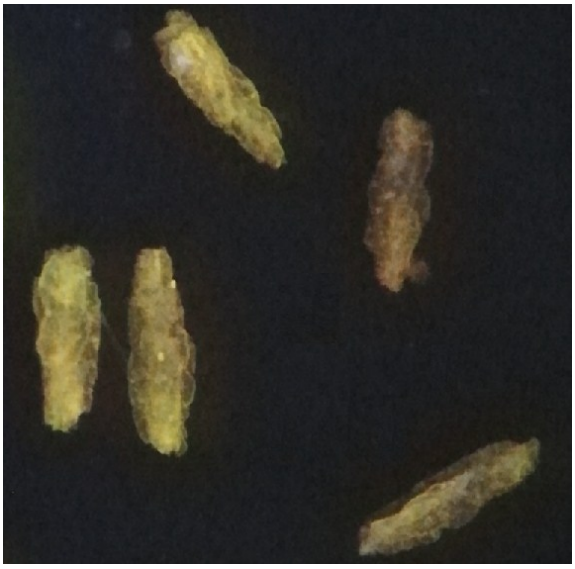

Figure S20. Photography of homogeneous yellow luminescent ***IAM19-1c'*** (Eu^{3+}, Tb^{3+}, Ce^{3+}-MOF) taken by ordinary microscope under the excitation of 254 nm.

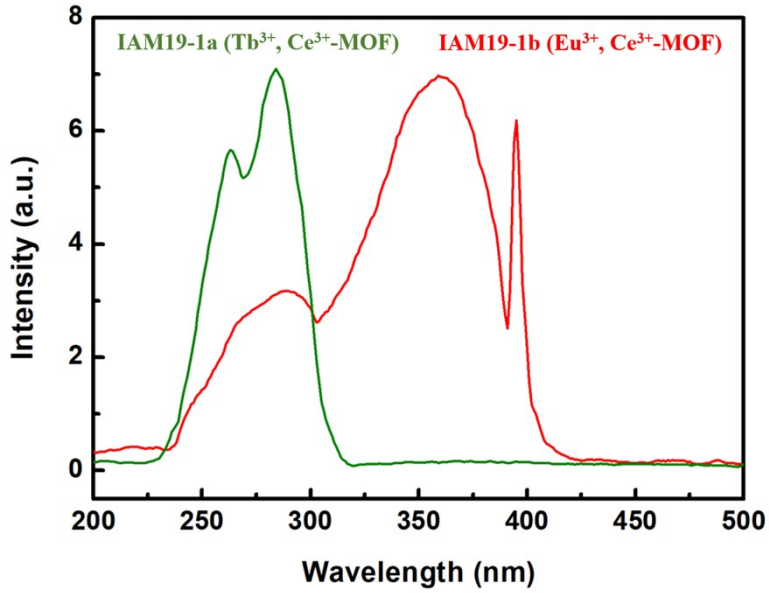

Figure S21. Excitation spectra of ***IAM19-1a*** (green, λ_{em}=543) and ***IAM19-1b*** (red, λ_{em}=617).

The spectra demonstrate that the energy transfer from Ce^{3+} to Tb^{3+} is more sensitive while the intrinsic excitation of Eu^{3+} (396 nm, $^7F_0 \rightarrow {}^5L_6$ transition of Eu^{3+}, represented by the red line) is stronger than that of Tb^{3+} (represented by the green line).

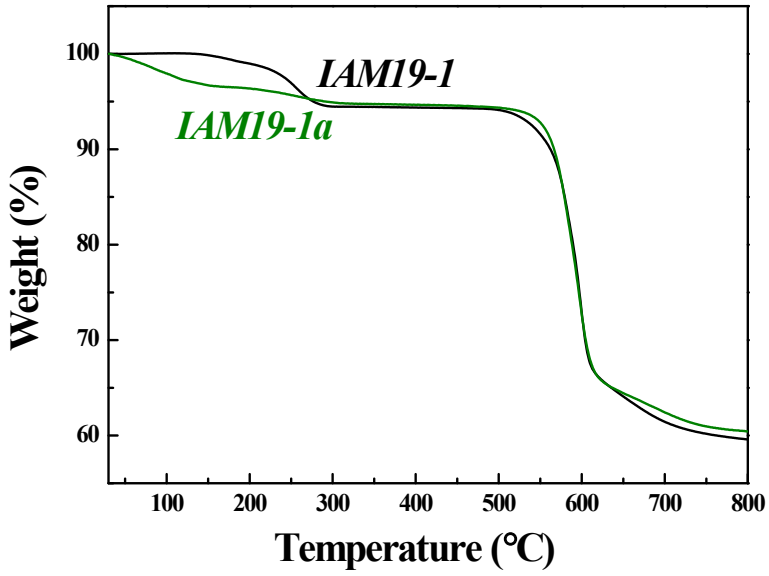

Figure S22. The TGA curves of ***IAM19-1a*** (green) and ***IAM19-1*** (black).

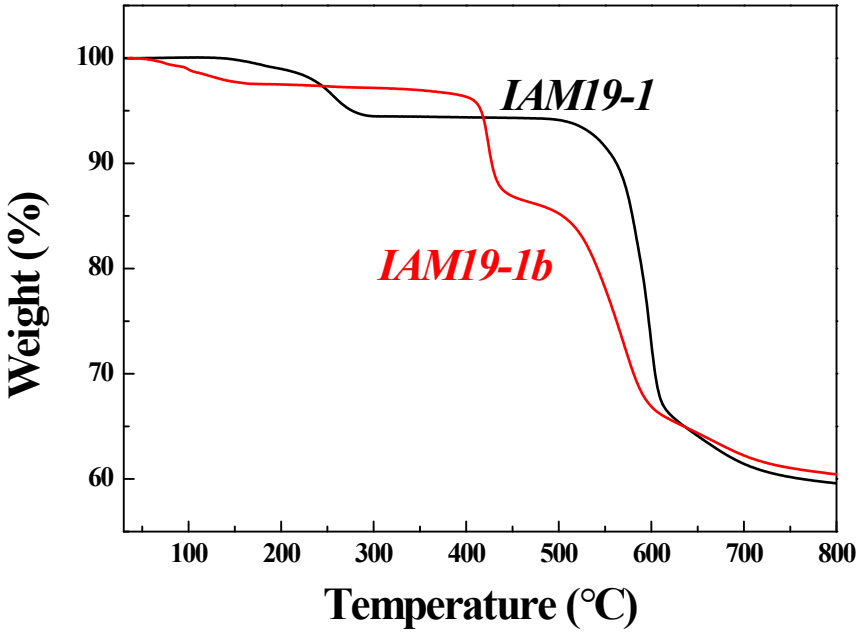

Figure S23. The TGA curves of ***IAM19-1b*** (red) and ***IAM19-1*** (black).

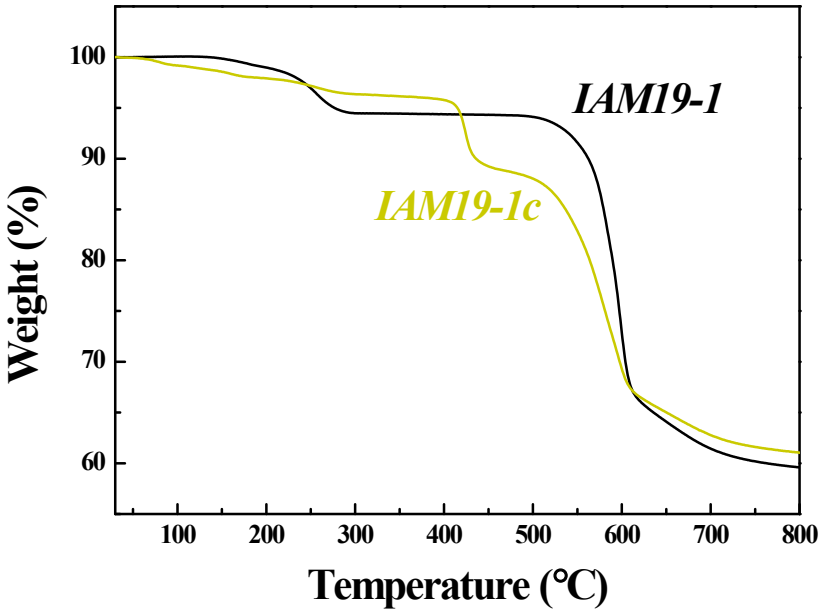

Figure S24. The TGA curves of ***IAM19-1c*** (yellow) and ***IAM19-1*** (black).